The EMBO Journal vol.13 no.17 pp.3953-3963, 1994

Use of photoaffinity crosslinking and molecular modeling to analyze the global architecture of ribonuclease P RNA

Michael E.Harris[1], James M.Nolan[1], Arun Malhotra[2,3], James W.Brown[1,4], Stephen C.Harvey[2] and Norman R.Pace[1,4]

[1]Department of Biology and Institute for Molecular and Developmental Biology, Indiana University, Bloomington, IN 47405 and [2]Department of Biochemistry and Molecular Genetics, Schools of Medicine and Dentistry, University of Alabama at Birmingham, Birmingham, AL 35294, USA

[3]Present address: The Rockefeller University, 1230 York Avenue, New York, NY 10021-6399, USA

[4]Present address: Department of Microbiology, North Carolina State University, Raleigh, NC 27695, USA

[5]Corresponding author

Communicated by J.A.Steitz

Bacterial ribonuclease P (RNase P), an endonuclease involved in tRNA maturation, is a ribonucleoprotein containing a catalytic RNA. The secondary structure of this ribozyme is well established, but comparatively little is understood about its 3-D structure. In this analysis, orientation and distance constraints between elements within the *Escherichia coli* RNase P RNA–pretRNA complex were determined by intra- and intermolecular crosslinking experiments. A molecular mechanics-based RNA structure refinement protocol was used to incorporate the distance constraints indicated by crosslinking, along with the known secondary structure of RNase P RNA and the tertiary structure of tRNA, into molecular models. Seven different structures that satisfy the constraints equally well were generated and compared by superposition to estimate helix positions and orientations. Manual refinement within the range of conformations indicated by the molecular mechanics analysis was used to derive a model of RNase P RNA with bound substrate pretRNA that is consistent with the crosslinking results and the available phylogenetic comparisons.

Key words: crosslinking/ribozyme/RNA tertiary structure/RNase P/transfer RNA

Introduction

Bacterial ribonuclease P (RNase P) RNAs constitute one class of catalytic RNA molecules (Altman *et al.*, 1993; Cech, 1993). During tRNA maturation, RNase P carries out a site-specific endonucleolytic cleavage that generates the mature tRNA 5′ end. In bacteria, RNase P is composed of a single RNA of ~400 nucleotides and a small protein subunit of ~120 amino acids. *In vitro*, at high ionic strength the RNA alone is an accurate and efficient catalyst (Guerrier-Takada *et al.*, 1983). Understanding the means by which RNase P RNA recognizes substrate pretRNA and enhances the rate of hydrolysis of a specific phosphodiester bond demands knowledge of its structure. The secondary structure of RNase P RNA is now well-defined by phylogenetic covariation analysis (James *et al.*, 1988; Brown *et al.*, 1991; Haas *et al.*, 1994). The base-paired elements constitute a series of helices connected by less regularly structured 'single-strand' regions. Sequence comparisons identify a subset of helices, termed core helices, which are present in all bacterial RNase P RNAs and so are likely to be important in the function of this ribozyme. The active site of RNase P RNA is probably composed of conserved nucleotides located in a few separate regions of the RNA chain and brought together in the tertiary structure. To understand the roles of these structural elements in the function of this ribozyme, the 3-D organization of the RNA must be established.

Approaches for the analysis of the global architecture of large RNAs are limited. Detailed structures of tRNAs have been determined by X-ray crystallography (Kim *et al.*, 1974; Robertus *et al.*, 1974; Moras *et al.*, 1980; Westhof *et al.*, 1985), but attempts to crystallize and determine the structure of larger RNA molecules have proven unsuccessful (but see Doudna *et al.*, 1993). NMR has been used to explore the structures of small RNA motifs, for example stable tetraloops (Heus and Pardi, 1991; Varani *et al.*, 1991), internal loops (Wimberly *et al.*, 1993) and pseudoknots (Puglisi *et al.*, 1990). However, the redundancy of the nucleotides limits the usefulness of NMR in examining RNA molecules hundreds of nucleotides long. Models of large RNAs, such as 5S and 16S rRNA, and the core of auto-catalytic group I introns have been developed based on phylogenetic and experimental data (Brimacombe *et al.*, 1988; Stern *et al.*, 1988; Westhof *et al.*, 1989; Michel and Westhof, 1990; Malhotra and Harvey, 1994). Although inexact, such models provide useful frameworks for further experimentation and the interpretation of mutational and chemical modification data.

One experimental method for determining structural relationships between different portions of an RNA chain is chemical crosslinking. We have used previously a photoactivatable crosslinking agent, the azidophenacyl (APA) group, specifically attached to the 5′ and 3′ termini of tRNA, to determine sites in RNase P RNA that interact with those elements of the substrate (Burgin and Pace, 1990; B.-K.Oh and N.R.Pace, manuscript submitted). The termini of RNAs are readily and specifically modified because of their unique chemical groups. Photoaffinity crosslinking agents can be coupled to locations that are normally interior in the RNA chain with the specificity and efficiency of end modification by using circularly permuted RNAs (cpRNAs) (Nolan *et al.*, 1993). cpRNAs retain the native RNA sequence but have their 5′ and 3′ ends relocated in the folded structure of the RNA. The

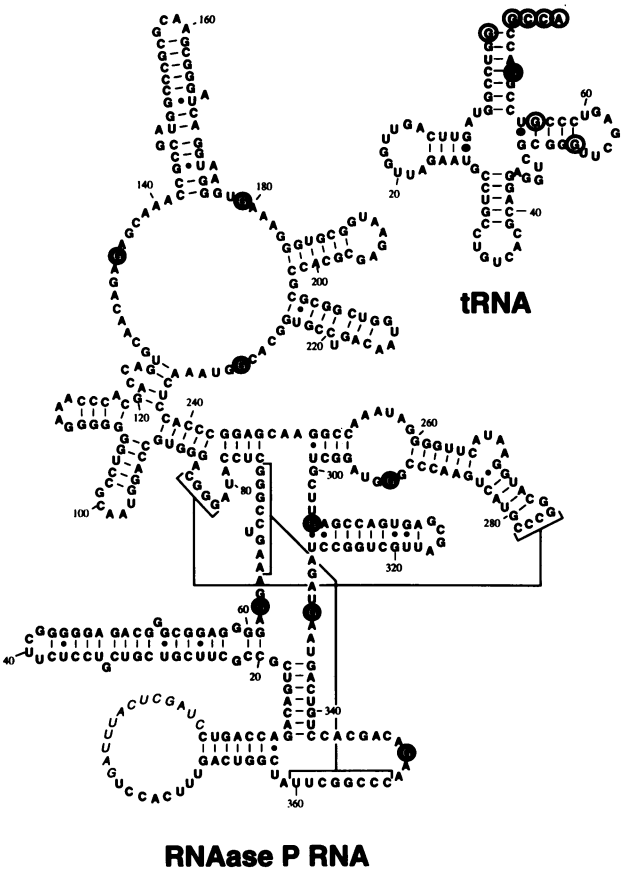

Fig. 1. Locations of photoagent attachment sites in RNase P RNA and $tRNA^{Asp}$. The secondary structures of *E.coli* RNase P RNA and *Bacillus subtilis* $tRNA^{Asp}$ are shown with photoagent attachment sites circled. Sites described in this study are indicated by filled circles, while previously described attachment sites on $tRNA^{Asp}$ are shown as open circles. tRNA is numbered according to Gauss *et al.* (1979). The numbering of RNase P RNA is that of the native sequence. Non-native nucleotides included in the cpRNase P RNAs are italicized. The linker connecting the 5′ and 3′ ends of $cptRNA^{Asp}$ has been described previously (Nolan *et al.*, 1993). Two long-range pairings in the *E.coli* secondary structure are indicated by brackets connected by lines.

results of intermolecular crosslinking using such photoagent-containing tRNAs identify elements of RNase P RNA which are juxtaposed to the sites of photoagent attachment in pretRNA while in the ribozyme–substrate complex. The results also establish specific distance constraints for generating molecular models. In this study the collection of distance constraints in the RNase P RNA–pretRNA complex is significantly extended by analysis of intramolecular crosslinking with eight different circularly permuted RNase P RNAs (cpRNase P RNAs) and intermolecular crosslinking using one additional cptRNA. The results obtained, together with the established secondary structure of RNase P RNA and tertiary structure of tRNA, were used with a molecular mechanics protocol to develop a model of the global structure of the core of the RNase P RNA–pretRNA complex. The experimental approach is applicable to the study of large-scale structure in other large RNAs.

Results

Design and catalytic properties of circularly permuted Escherichia coli RNase P RNAs

Eight different cpRNase P RNAs were constructed to provide specific photoagent attachment sites for intramolecular crosslinking (Figure 1). The locations of the new endpoints in the cpRNase P RNAs were selected primarily by their strategic positions; however, the use of phage T7 RNA polymerase for *in vitro* transcription dictated that the RNAs initiate with a guanosine residue (Milligan and Uhlenbeck, 1989). Some of the attachment sites (Ec179, Ec292, Ec332) are at, or near, nucleotides protected from chemical modification in the presence of tRNA (Knap *et al.*, 1990; LaGrandeur *et al.*, 1994). Others (Ec63, Ec229, Ec292, Ec332, Ec350) are at, or adjacent to, sites which crosslink to photoagent-modified tRNA (Burgin and Pace, 1990; Nolan *et al.*, 1993; B.-K.Oh and N.R.Pace, manuscript submitted). All of the attachment sites are located in conserved sequences and thus are expected to provide structural information on the functional core of the ribozyme. Additionally, one cptRNA was constructed (5′ end at G69, termed cptRNA69) for use in intermolecular crosslinking (Figure 1). Circularly permuted DNA templates for transcription were amplified by PCR from a plasmid containing tandemly repeated genes (Nolan *et al.*, 1993). Oligodeoxynucleotide primers dictate the endpoints of a particular template DNA and thus the 5′ and 3′ ends of the transcribed RNA.

Table I. Catalytic activity of cpRNase P RNAs

RNase P RNA	k_{cat} (min^{-1})	K_m (μM)
Native[a]	0.670 ± 0.210	0.072 ± 0.030
Ec63[a]	0.512 ± 0.163	0.082 ± 0.025
Ec135	0.576 ± 0.194	0.207 ± 0.063
Ec179	0.922 ± 0.211	0.104 ± 0.057
Ec229	0.970 ± 0.330	0.063 ± 0.003
Ec292[a]	37.400 ± 4.400	1.400 ± 0.300
Ec304[a]	0.565 ± 0.336	0.045 ± 0.006
Ec332	0.544 ± 0.300	0.152 ± 0.061
Ec350[a]	0.268 ± 0.077	0.070 ± 0.029
cptRNA 69	0.150 ± 0.100	0.052 ± 0.004

[a]Kinetic parameters determined at 3 M ammonium acetate.

cpRNAs are expected to form the native structure, but contain a nick. Discontinuities in the ribose phosphate backbone do not appear to alter significantly the catalytic activity of RNase P RNA (Reich *et al.*, 1986; Guerrier-Takada and Altman, 1992; Waugh and Pace, 1993), indicating that the structure is maintained by secondary and tertiary interactions. Nevertheless, it was important to establish that the cpRNAs studied here accurately reflect the native RNA structures. This is indicated by their participation in the RNase P reaction. As shown in Table I, the kinetic parameters k_{cat} and K_m for the cpRNAs used in this study are approximately the same as those of their native counterparts. Several of the cpRNase P RNAs (Ec63, Ec304, Ec350) displayed slightly (<10-fold) higher K_m values than the native RNA at 1 M monovalent salt, but exhibited near-native kinetic parameters at a higher concentration of monovalent cation (3 M) (Table I and data not shown). Since the rate of the *in vitro* RNase P RNA reaction is limited by release of product (Reich *et al.*, 1988; Tallsjö and Kirsebom, 1993), increases in K_m also result in elevated k_{cat} values. The reduced affinity for substrate (increase in K_m) exhibited by some of the cpRNase P RNAs probably reflects an increased flexibility in the RNase P RNA chain due to interruption of the phosphodiester backbone. The high concentration of

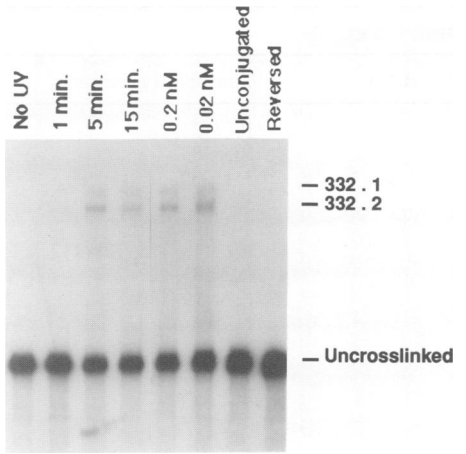

Fig. 2. Analysis of intramolecular crosslinking of 5′-APA Ec332 cpRNase P RNA. Radiolabeled 5′-APA Ec332 cpRNase P RNA was incubated under *in vitro* RNase P RNA reaction conditions: 1 M ammonium acetate, 40 mM Tris−HCl, pH 8.0, 25 mM $MgCl_2$, 0.1% SDS. The lane marked 'No UV' was not exposed to 302 nM light, while the lanes marked '1 min', '5 min' and '15 min' were irradiated for those lengths of time. The concentration of 5′-APA Ec332 RNA was 2 nM unless otherwise indicated. The time of irradiation of the 'Reversed' and 'Unconjugated' samples was 30 min. After crosslinking, the 'Reversed' sample was treated with phenyl mercuric acetate, which cleaves the thioester bond linking the crosslinking reagent to the 5′ end of 332 cpRNase P RNA (Neumann and Smith, 1967). The 'Unconjugated' sample contains RNA which was not modified with the APA photoagent.

monovalent cation suppresses the effect of the nick presumably by screening repulsive forces which work to distort the cpRNA from its native structure. The crosslinking studies outlined below were performed under the optimal catalytic conditions for each cpRNA.

Crosslinking of 5′-APA cpRNAs in the ribozyme−substrate complex: analysis of intra- and intermolecularly crosslinked species

For crosslinking, an APA group was attached to the 5′ ends of cpRNAs containing a 5′ phosphorothioate (Burgin and Pace, 1990) incorporated during transcription. Inclusion of guanosine monophosphorothioate in transcription reactions results in its incorporation only at the 5′ end, since nucleoside monophosphates can initiate transcription but are unable to be utilized for elongation by T7 RNA polymerase (Milligan and Uhlenbeck, 1989). The phosphorothioate sulfur provides a unique site in the RNA for the attachment of the APA group. Irradiation with 302 nm light converts the azido group to a highly reactive nitrene which is able to insert into a variety of covalent bonds (Hixson and Hixson, 1975; Schuster and Platz, 1992).

Intramolecular crosslinking of 5′-APA cpRNAs results in the formation of lariats which can be separated from uncrosslinked RNA by PAGE. Figure 2 documents intramolecularly crosslinked species formed by 5′-APA Ec332 RNA. Crosslinked species appear as bands migrating more slowly than the uncrosslinked RNA. Crosslinking for all 5′-APA cpRNase P RNAs was rapid, occurring with a $t_{\frac{1}{2}}$ of <5 min (Figure 2 and data not shown). Crosslinking occurs exclusively via the APA moiety at the 5′ end since unconjugated RNA did not form crosslinks, and cleavage of the thioester linkage between the RNA and the photoagent with phenyl mercuric acetate (Neumann and Smith, 1967) eliminated the slowly migrating lariats. The intramolecular nature of the crosslinks is indicated by the insensitivity of the reaction to dilution; no decrease in the conversion to crosslinked RNA was seen when the concentration of conjugated RNA was reduced 1000-fold (Figure 2 and data not shown).

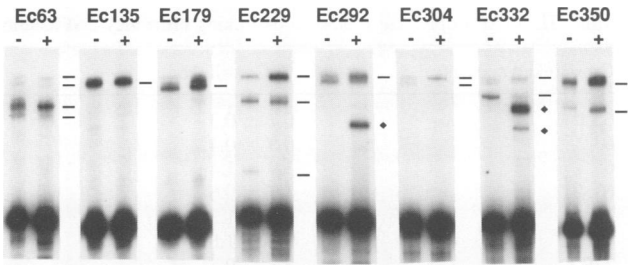

Fig. 3. Identification of crosslinked species. Radiolabeled 5′-APA cpRNase P RNAs at 2 nM were irradiated with 302 nM light for 15 min in either the presence (+) or absence (−) of 100 nM pretRNA. The reaction conditions are those described in Table I, except that $CaCl_2$ was substituted for $MgCl_2$ (Smith and Pace, 1993). The presence of $CaCl_2$ slows the catalytic rate without affecting pretRNA binding so that the amount of pretRNA cleavage during the crosslinking reaction was undetectable. Lines to the right of each pair of lanes indicate the major crosslinked species. Filled diamonds indicate the position of pretRNA-specific crosslinked species.

Figure 3 shows the crosslinking results obtained with all eight cpRNase P RNAs, alone and in the presence of substrate pretRNA. Individual crosslinked species are designated numerically beginning with the species migrating most slowly in the gel (for example the upper band in Figure 2 is denoted as 332.1 and the lower as 332.2). The conversion of RNA containing the photoagent into crosslinked species was efficient, between 0.7 and 8.0% (Table II). The presence of substrate resulted in only small changes in the pattern of crosslinked species with a few of the photoagent-modified RNase P RNAs. For example, 5′-APA Ec63 formed four different crosslinked species in the absence of pretRNA (Figure 3). The same crosslinked species were produced in the presence of pretRNA, but the conversion of one species, 63.3, increased by 30%. Similar small (<2-fold) increases in the conversion into crosslinked species 179.1 and 229.1 occurred in the presence of pretRNA (Table II). The conversion into 229.2 and 332.2 decreased in the presence of tRNA. Two species, 229.3 and 304.2, were eliminated upon addition of tRNA. Increases in the conversion into particular crosslinked species is likely due to stabilization of the RNase P RNA structure when complexed with substrate. Decreased conversion in the presence of substrate could be due to either solidification of the structure, which might restrict the range of the photoagent, or occlusion of the crosslink site by pretRNA.

Crosslinked species were observed with Ec292 and Ec332 in the presence of substrate that did not occur with those cpRNase P RNAs alone (Figure 3). These pretRNA-specific species could be due to the formation of new intramolecular crosslinks or to intermolecular crosslinking between RNase P RNA and bound pretRNA. Crosslinking reactions with radiolabeled pretRNA and non-radiolabeled Ec292 or Ec332 RNA demonstrated that the pretRNA was incorporated into crosslinked species 292.2, 332.3 and 332.4 (data not shown), which therefore constitute intermolecular crosslinks. Since no new intramolecular

Table II. 5′-APA cpRNase P RNA crosslinking efficiency and location of crosslinked nucleotides

Crosslinked species	% Crosslinked	% Crosslinked + tRNA	Crosslinked nucleotides
63.1	0.7 ± 0.3	0.9 ± 0.4	10–11, 15
63.2	0.8 ± 0.4	0.9 ± 0.4	363–365
63.3	3.9 ± 1.4	6.0 ± 2.7	351, 352
63.4	1.7 ± 0.6	1.8 ± 0.6	335
135.1	4.5 ± 1.3	5.1 ± 1.2	112, 118
179.1	3.6 ± 1.6	6.2 ± 2.1	112, 118, 123, 128–132
229.1	2.8 ± 0.7	6.9 ± 1.6	183–185, 227–228
229.2	5.8 ± 1.8	4.3 ± 1.2	127–129, 137–138
229.3	2.5 ± 0.6	–	1, 386
292.1	6.4 ± 1.9	6.0 ± 1.7	247–248, 253–255, 258–260
292.t1[a]	–	7.2 ± 1.9	+2, +3 (pretRNA)[b]
304.1	1.2 ± 0.2	1.3 ± 0.2	295–296
304.2	1.1 ± 0.2	–	247–248
332.1	1.7 ± 0.5	1.3 ± 0.3	295
332.2	4.7 ± 0.6	2.1 ± 0.7	246–248
332.t1[a]	–	8.7 ± 1.3	−4, −5 (pretRNA)[b]
350.1	5.4 ± 0.4	6.1 ± 0.6	300, 329–330
350.2	1.8 ± 0.6	2.6 ± 0.4	246–248

[a]Intermolecular crosslink to pretRNA.
[b]Numbering relative to RNase P RNA cleavage site.

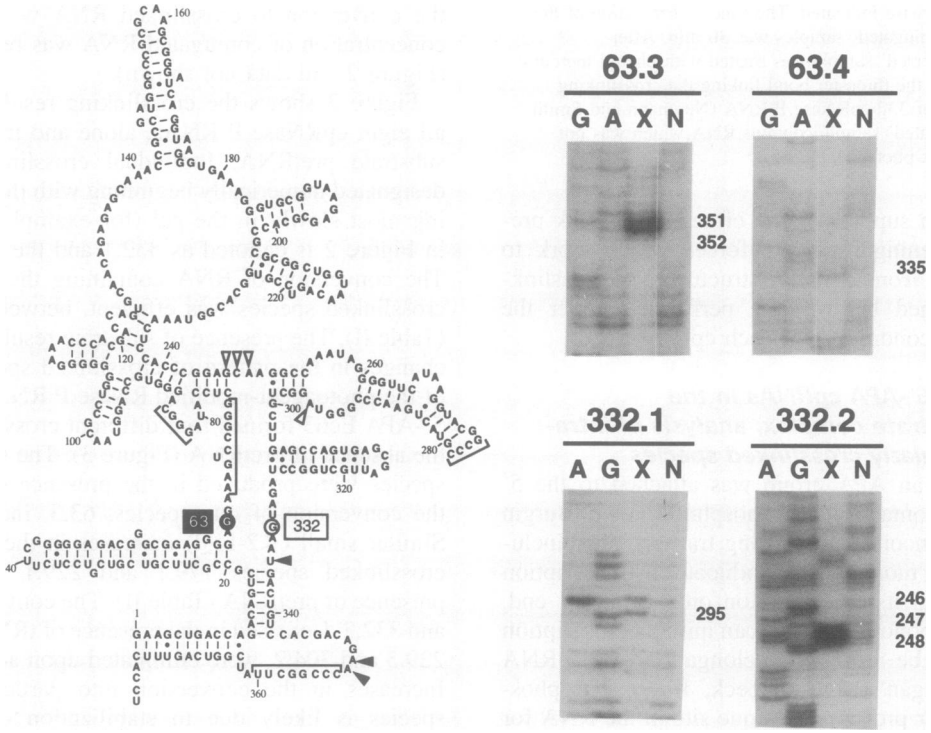

Fig. 4. Mapping of Ec332 and Ec63 5′-APA cpRNase P RNA intramolecular crosslinks by primer extension. The location of the Ec332 and Ec63 photoagent attachment sites are indicated by circled nucleotides on the *E.coli* secondary structure. The filled circle indicates the position of the Ec63 attachment site and the open circle indicates the position of the Ec332 attachment site. Filled arrows indicate the position of nucleotides in the major crosslinked species formed using 5′-APA Ec63 RNA and open arrows indicate crosslinked nucleotides detected using 5′-APA Ec332 RNA. The primer-extension reactions are shown on the right. Lanes marked G, A and N denote lanes containing G and A sequencing reactions and a control primer extension with uncrosslinked RNA, respectively. Lanes marked X contain the products of a primer-extension reaction using the crosslinked species indicated above each gel. The nucleotide positions indicated correspond to the crosslinked sites, the nucleotides 5′ in the template from the sites of termination of primer extension.

crosslinks are observed in the presence of pretRNA, and only small changes are seen in the pattern of crosslinked species upon substrate binding, it appears that no major changes in RNase P RNA conformation take place upon pretRNA binding. It remains possible that the photoagent attachment sites used in this study are not in positions which could detect substrate-induced conformational shifts. However, this seems unlikely considering the extensive distribution of photoagents in the structural core of the molecule.

The particular nucleotides crosslinked to the 5′ ends of the cpRNase P RNAs were determined by primer-extension mapping. Individual crosslinked species were gel-purified and used as templates for primer-extension reactions with

Table III. Intermolecular crosslinking results using photoagent-modified tRNA probes

Modified tRNA nt	RNase P RNA crosslink sites	Reference
1	248, 249, 330–333	Burgin and Pace (1990)
53	111–114, 348, 349	Nolan *et al.* (1993)
64	64–67, 77, 78, 98–101,118, 247–249	Nolan *et al.* (1993)
69	10, 64–67, 192, 248, 252, 253, 332–334, 341–344	this study
73	253, 254, 293, 294, 296, 297, 331–333	B.-K.Oh and N.R.Pace, submitted
76	259–261, 285–287, 290, 292	B.-K.Oh and N.R.Pace, submitted

reverse transcriptase. Reverse transcriptase terminates one nucleotide 3′ to crosslink sites in the RNA template [Burgin and Pace (1990) and references therein]. Examples of this analysis for the major Ec63 and Ec332 crosslinked species are shown in Figure 4. Comparison of extension products from crosslinked RNA with reaction products from uncrosslinked RNA and sequencing reactions identifies the individual crosslinked nucleotides. Table II lists the sites of crosslinking in all of the species detected in Figure 3. In each case the locations of the crosslink sites in the cpRNA corresponded to the relative migration of the crosslinked species on polyacrylamide gels. Crosslinking of the photoagent located at the 5′ end of the RNA to sequences near the 3′ end resulted in species which migrated higher in the gel than crosslinking to sequences more 5′-proximal. For example, crosslinking of 5′-APA Ec332 to A295 was detected as crosslinked species 332.1, which migrated more slowly than 332.2 in which the 5′ end was crosslinked to G246, C247 and A248. Thus, the electrophoretic properties of the different crosslinked species offer some corroboration of the primer-extension results.

Three crosslinked species observed only in the presence of pretRNA (292.2, 332.3 and 332.4) were identified as resulting from intermolecular crosslinking (above). In these cases the crosslinked nucleotides in pretRNA were identified using oligonucleotides for primer extension that were specific to tRNA sequences (Table II). Other intermolecular crosslinking results obtained using modified tRNA are described elsewhere (Burgin and Pace, 1990; Nolan *et al.*, 1993; B.-K.Oh and N.R.Pace, manuscript submitted) and are summarized in Table III. One additional cptRNA (5′ end at G69) was used to probe RNase P RNA structure in intermolecular crosslinking experiments. This cptRNA was an efficient substrate for native RNase P RNA (Table I) and crosslinked with high efficiency (3% conversion) to native *E.coli* RNase P RNA (data not shown). The crosslinking results obtained with cptRNA69 are also summarized in Table III.

It is possible that some of the crosslinks detected represent alternative non-active structures. The degree of catalytic activity of all of the cpRNase P RNAs indicates that inactive conformations are not engendered by circular permutation. We have tested directly the crosslinked species derived from Ec135, Ec292 and Ec332 cpRNAs, all of which retained catalytic activity. Moreover, all of the intermolecular crosslinks detected with 5′-APA RNase P RNA retained catalytic activity; incubation of the conjugates under reaction conditions resulted in cleavage of the crosslinked substrate (M.E.Harris and N.R.Pace, unpublished results). The fact that no mutually exclusive crosslinking results are observed (see below) also suggests that we are probing the native RNase P RNA structure.

Within the library of positional information (Tables II and III) much of the data are complementary in nature. For example, 5′-modified tRNA crosslinks to nucleotides 248, 249 and 330–333 indicating that these nucleotides are near to the pretRNA cleavage site, and each other, in the ribozyme–substrate complex (Table III; Burgin and Pace, 1990). Intramolecular crosslinking with 5′-APA Ec332 also indicates that G332 and A248 are nearby in the RNase P RNA structure (Table II). Intermolecular crosslinking to pretRNA nucleotides −4 and −5 (just upstream of the cleavage site) was detected with 5′-APA-Ec332 RNase P RNA. The intermolecular crosslinking data with tRNA modified at position one had already established that RNase P RNA nucleotide G332 was in the vicinity of the pretRNA cleavage site. Furthermore, modification–interference studies have shown that G332 is protected from modification in the presence of precursor, but not mature tRNA (LaGrandeur *et al.*, 1994). This suggests the proximity of G332 and precursor-specific sequences. In some cases, crosslinking that might have been expected based on previous experiments did not occur. pretRNAs modified at either positions 64 or 69 crosslinked in the vicinity of RNase P RNA nucleotide G63; however, no reciprocal intermolecular crosslinking was observed using 5′-APA Ec63. This could be due to differences in the directionality of the photoagent when placed at these different locations. Nevertheless, 5′-APA Ec63 did form intramolecular crosslinks to nucleotides that are at (A10) or adjacent to (U335 versus U334) positions crosslinked with photoagent-modified cptRNA69.

Global architecture of the RNase P RNA–pretRNA complex

A molecular mechanics-based RNA structure refinement protocol (Malhotra *et al.*, 1990, 1994) was employed to incorporate the crosslinking data, the secondary structure of RNase P RNA and the tertiary structure of tRNA into coherent molecular models of the RNase P RNA–pretRNA complex. The secondary structure and extensive crosslinking data outlined in Tables II and III are insufficient to specify a unique 3-D model in atomic detail. Therefore we use a reduced representation (one pseudo-atom = one nucleotide) that more accurately represents the available structural data. Positional constraints indicated by the secondary structure and the crosslinking information were imposed by a series of bonds, angles and torsions which are enforced on a series of randomly generated starting conformations by energy minimization and dynamics. Crosslinking constraints take the form of pseudobonds with an ideal distance of 10 Å, corresponding to the length of the APA photoagent. The mature portion of pretRNA^{Asp} was forced to adopt the conformation

determined by X-ray crystallographic analysis (Westhof and Sundaralingam, 1986). Helices which are contiguous in the secondary structure were initially modeled as stacked, based on stacking arrangements in tRNA and group I introns (Michel and Westhof, 1990).

At the current level of resolution the molecular mechanics results are most usefully compared in the context of helix position and orientation. Seven similar models satisfying all of the input constraints emerged from the molecular mechanics analysis and constitute a survey of available conformations fitting the data [Figure 5; the nomenclature used to refer to individual helices is that of Haas *et al.* (1994)]. Average helix positions and orientations were calculated after superposition (Figure 5B), maximizing the overlap of a subset of the core helices (P2, P4, P7, P8 and the acceptor and TΨC stems of tRNA). The standard deviations from these average positions (Figure 5C) give some indication of the differences in models generated with this set of structural data. The use of different subsets of core helices for superposition resulted in similar average helix positions and standard deviations (data not shown). The positions of several of the core helices have standard deviations of <7 Å (P4, P5 and P7–P9). Other core helices (P3 and P18) have standard deviations >10 Å and so are more poorly constrained by the available structural data.

The positions of helices P12, P13 and P14 display the greatest standard deviations (>15 Å) and so their average positions are less informative. Many of the crosslinks detected in this region involve unbase-paired nucleotides. The additional degrees of freedom allowed 'single-stranded' regions in our modeling protocol results in the higher standard deviations in these helix positions. Thus P12, P13 and P14 were excluded from further structural analysis (see below). Since deletion of these helices from *E.coli* RNase P RNA results in a ribozyme with catalytic efficiency (k_{cat}/K_m) within 10-fold of the native RNase P RNA value (R.Siegel and N.R.Pace; unpublished results), this exclusion has little impact on our view of the RNase P RNA structure required for function.

The average helix positions indicated by the molecular mechanics analysis (Figure 5D) provide a global view of RNase P RNA–pretRNA interaction. This representation should be interpreted cautiously, as it presents average helix positions rather than an average composite model for the RNase P RNA. P7–P10 are positioned at the distal end of the tRNA acceptor stem near the TΨC loop. This is indicated by the extensive crosslinking between tRNA nucleotides G64 and G54 and this region of RNase P RNA (Table III; Nolan *et al.*, 1993). However, the precise orientation of these helices is uncertain. Helices P1, P2 and P3 and helices P15, P16 and P18 appear to be positioned on opposite sides of the substrate pretRNA (Figure 5D). This arrangement is indicated by the intermolecular crosslinks from tRNA nucleotide G69 to nucleotides in P1 (C10) and P2 (U341 and C342) of RNase P RNA. Additionally, crosslinking from RNase P RNA nucleotide G292 (near P15) to pretRNA nucleotides +2 and +3, which are on the opposite side of the tRNA acceptor stem from +69, supports this arrangement. P4 and P5, which connect the P1–P2–P3 and P15–P16–P18 domains, are located near the pretRNA cleavage site (consistent with the presence of conserved sequences in P4) and oriented perpendicular to the axis of the tRNA acceptor stem (Figure 5D).

Discussion

This study extends significantly the library of positional information on the structure of the RNase P RNA–pretRNA complex. Application of this information with a molecular mechanics computer modeling protocol designed to survey conformations consistent with the available data provides a global view of helix positions in the complex. The positions of most of the core helices in the collection of models display standard deviations that are <10 Å from their average position. To derive a single structure model reflecting the phosphodiester backbone, we constructed a manual model based on the molecular mechanics results and other considerations.

In the manual assembly of a model of the RNase P RNA–pretRNA core structure based on the crosslinking and molecular mechanics results, the RNase P RNA portion of the complex was initially taken as three structural domains: P1–P5, a cruciform structure comprised of P7–P10 and a third domain composed of P6 and P15–P18. Because of their proximity in the secondary structure, P1–P3 were modeled as forming a continuous coaxial stack. The P1 and P3 helices vary in length between RNase P RNAs from different organisms, while the length of P2 is conserved (Brown *et al.*, 1991). This is consistent with a continuous P1–P2–P3 helical array in which the ends can vary in length, while the positions of the junctions between these helices and the rest of RNase P RNA remain fixed. Also, considering their proximity in the secondary structure, P4 and P5 were taken as a continuous helical stack.

P7, P8, P9 and P10 form a four-helix junction in the secondary structure. Based on the structure of such junctions in DNA oligomers (Cooper and Hagerman, 1989; Murchie *et al.*, 1989), we model this junction as a cruciform. In this arrangement only two stacking conformations are geometrically feasible: a P7–P8 stack and a P9–P10 stack, or alternatively a P7–P10 stack and a P8–P9 stack. Since the bulged nucleotide A118 in P9 and nucleotides in the P8 loop are both crosslinked by a photoagent attached to G64 on tRNA (Nolan *et al.*, 1993), the P7–P10/P8–P9 conformation was chosen for the model. This arrangement brings A118 and the loop of P8 closer together (as expected from the crosslinking data) than the alternative arrangement.

P15 and P16 and the internal loop connecting them are modeled as a continuous helical element. The structure of the internal loop between the P15 and P16 helices is unknown. While the pairing across this region is likely to be complex, it is reasonable to assume, based on the structures of other internal loops (Holbrook *et al.*, 1991; Wimberly *et al.*, 1993), that the orientation of the phosphodiester backbone in this region is approximately helical. This region was modeled as an A-form helix in the molecular mechanics analysis. This is no doubt an oversimplification, but it seems more appropriate than allowing these sequences as much flexibility as single-stranded regions. An acute angle between the axis of P16 and P17 is necessary to accommodate the P6 pairing, since the base of P15 is fixed in the secondary structure nearby P6.

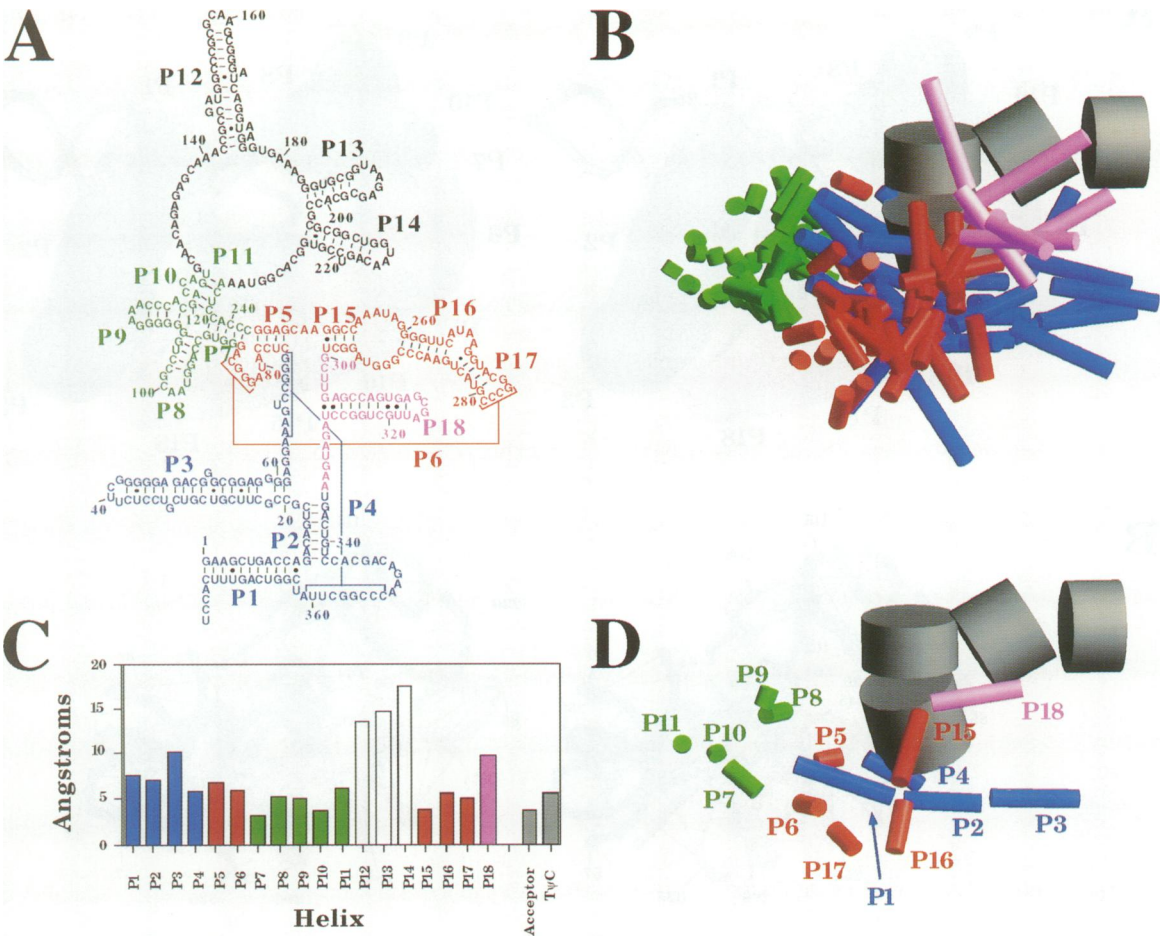

Fig. 5. Molecular mechanics computer modeling of the RNase P–pretRNA complex. (**A**) Secondary structure of *E.coli* RNase P RNA. Helices are designated according to Haas *et al.* (1994). Colors correspond to the helical cylinder representations in (B) and (D). (**B**) Superposition of seven different models of *E.coli* RNase P RNA derived by molecular mechanics. The different models were superimposed based solely on the position of tRNA. tRNA helices are displayed as gray cylinders with their diameters proportional to ideal A-RNA helix width. Blue, red and green cylinders denote RNase P RNA helices P1–P11 and P15–P18 and correspond in color to the secondary structure shown in (A). RNase P RNA helices are shown as cylinders with diameters 20% that of helix width but with the appropriate length of the actual helices. RNase P RNA helices from seven different structures derived by molecular mechanics are shown. (**C**) Variation in the positions of helical segments, as measured by standard deviation in the position of helix midpoints, for the seven models derived using the molecular mechanics protocol. The standard deviation, in Å, is indicated by columns. The data for the D-loop stem and anticodon stem of tRNA are omitted. (**D**) Average helical positions and orientations indicated by the molecular mechanics computer modeling. The range of potential physical models is suggested by the standard deviations in (C). tRNA and RNase P RNA helices are displayed as in (B). The identities of individual helices are indicated.

This 'elbow' between P16 and P17 can vary greatly in sequence and structure in different bacterial RNase P RNAs, often with additional helices interposed between P16 and P17 (Brown *et al.*, 1991). The sequence-length variability in this region is consistent with a location of P15 and P6 proximal to the catalytic core, and the connection between P16 and P17 forming a U-turn of the phosphodiester backbone. The variability in sequence-length and structure suggest that this connection lies on the exterior of the molecule.

During manual refinement the following alterations from the average helix positions indicated by the molecular mechanics analysis (Figure 5D) were made.

(i) The P1–P2–P3 element was rotated to remove P1 from the interior of the molecule. P1 varies in length between different bacterial RNase P RNAs, and is therefore unlikely to be oriented into the interior of the structure. This rotation satisfies the important (high efficiency) intermolecular crosslinks between pretRNA nucleotide 69 and the P1–P2–P3 element (C10, U341 and C342) by avoiding the location of P4 between these crosslinking nucleotides which occurred in a few of the structures derived by molecular mechanics. As shown in Figure 5C, the standard deviations for the positions and orientations of helices P1, P2 and P3 are relatively high compared with other structural elements, and thus only their approximate location relative to pretRNA can be modeled at this time.

(ii) The P15, P16 and P18 helices were positioned underneath the substrate pretRNA rather than directly beside it, as indicated by the average helix positions. If the P16–P15–P18 element was oriented beside the pretRNA, then crosslinks from tRNA nucleotide G69 to P15 (C253 and C252) would only be satisfied through the tRNA acceptor stem. Locating P15 below pretRNA allows an unobstructed path between tRNA nucleotide G69 and P15 (compare Figures 5D and 6A). In addition, this location of P15 satisfies high-efficiency crosslinks between the pretRNA 3′ end and the P15–P16 internal loop without reversing the direction of the pretRNA phosphodiester backbone, as would be necessary if P15 and P16 were

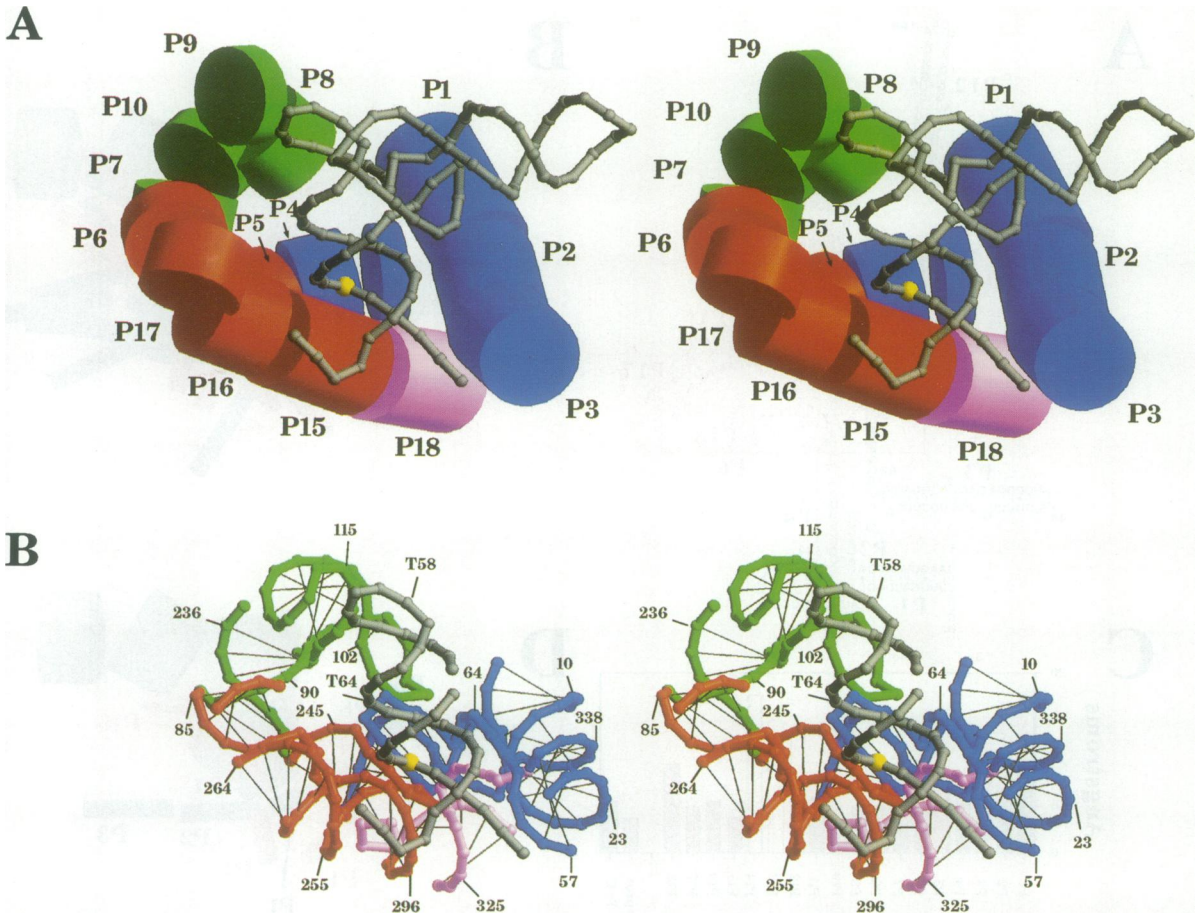

Fig. 6. Manually refined 3-D molecular model of the RNase P RNA–pretRNA complex based on molecular mechanics analysis. (**A**) Helix positions and orientations are displayed as cylinders of appropriate diameter and length. RNase P RNA helices are colored and numbered according to the secondary structure in Figure 5A. pretRNA is displayed as a series of cylinders connecting spheres which correspond to the position of individual nucleotides. The position of the mature tRNA 5′ end is shown as a yellow sphere. Helices P12, P13 and P14 are omitted as discussed in the text. The identities of individual helices are indicated. (**B**) Spheres represent the locations of individual nucleotides in RNase P RNA and pretRNA. The structure is colored according to the secondary structure in Figure 5A and numbered accordingly. For clarity the anticodon stem and D-loop stem of pretRNA and P17 of RNase P RNA are not shown. Only the proximal four base-pairs of P1, P3 and P18 are shown. Both representations are oriented as in Figure 5.

not located below the bound pretRNA. Another attractive feature of the positioning of P15, P16 and P18 is that in this orientation pretRNA interacts with a cleft in RNase P RNA rather than being surrounded by RNase P RNA helices. This configuration is consistent with modification–interference data, which suggest that only the surface of the acceptor stem that is distal to the anticodon loop interacts with RNase P RNA (Kahle *et al.*, 1990; Thurlow *et al.*, 1991). Because of the imposed stacking of P15 on P18, the location of P18 in the manually refined model is significantly different from the average helix positions indicated by molecular mechanics. However, the high standard deviation for the position of P18 in the collection of models makes it difficult to view the position of this helix with confidence at this time.

(iii) Helices P7–P10 were moved closer to the TΨC loop of tRNA. The P7–P10 element is well constrained by the available crosslinking data to a region near the TΨC loop of the tRNA acceptor stem, but the precise orientation of these helices could not be extracted from the molecular mechanics analysis. In fact, in some of the structures derived in the molecular mechanics analysis P4, P5 and P15 were positioned between P7–P10 and pretRNA. This results in average locations of P7–P10 in the molecular mechanics model which are relatively distant from the pretRNA compared with the distances in the manually refined structure. The crosslinking of pretRNA nucleotides G53 and G64 to the loops of P8 and P9, respectively, suggests that the angle between the axes of the acceptor stem helices and the P8–P9 stacked helices is small (Figure 6). Phylogenetic data are consistent with this arrangement in that P8 is oriented towards the interior of the refined structure model and P9 towards the exterior (Figure 7). The length of P8 varies only slightly (2–3 bp) between different bacterial RNase P RNAs, while P9 can increase dramatically in length (to >20 bp) (Brown *et al.*, 1991).

The arrangement of RNase P RNA core helices in the manually refined model has a number of attractive features. The conserved nucleotides indicated by phylogenetic comparisons are clustered in the core of the manually refined structure model and positioned in specific ways relative to the pretRNA cleavage site (Figures 6B and 7). This arrangement is consistent with the expectation that conserved sequences are involved in forming the active site of the enzyme. Another favorable comparative correlation

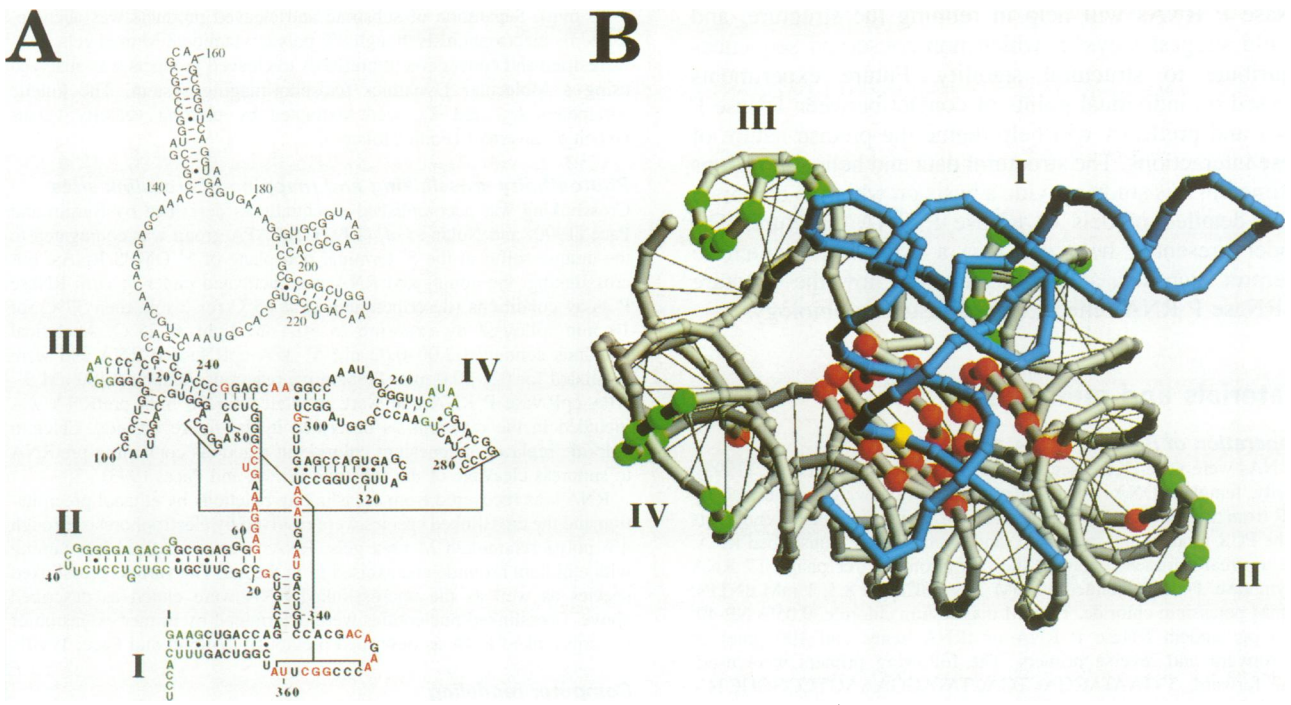

Fig. 7. Locations of conserved nucleotides and regions of sequence-length variation. Secondary structure (**A**) and manually refined 3-D model (**B**) of *E.coli* RNase P RNA. Nucleotides which are invariant among all known bacterial RNase P RNAs are shown in red. The locations of regions which vary in sequence length in different organisms are shown in green. pretRNA is shown in blue, with the location of the RNase P cleavage site shown as a yellow sphere. Roman numerals I–IV indicate the corresponding regions of sequence-length variation on both the secondary and tertiary structural models. The tertiary structure is oriented as in Figures 5 and 6.

with the structural model is that regions of RNase P RNA subject to length variation are on the exterior of the structure. Both the molecular mechanics modeling and the manually refined structure are consistent with the following basic arrangement of the conserved RNase P RNA nucleotides relative to the pretRNA cleavage site (Figure 6B). The major groove at the base of the tRNA acceptor stem faces the conserved sequences at the base of RNase P RNA P4 (nucleotides 62–69). The universally conserved RNase P RNA nucleotides A248 and A249 are positioned facing the minor groove at the base of the acceptor stem, adjacent to the substrate phosphodiester bond. RNase P RNA nucleotides 328–332 are positioned below the acceptor stem, appropriate for interaction with the precursor 5′ leader sequences. Both intra- and intermolecular crosslinking results place A248 and G332 in the vicinity of the pretRNA cleavage site (Tables I and II). The intermolecular crosslinking results using 5′-APA Ec332 (crosslinks to pretRNA positions −4 and −5 in the 5′ leader sequence) also support the idea that this region of RNase P RNA is where the 5′ leader sequences of pretRNA exit the ribozyme−substrate complex. Modification−interference studies have further shown that G332 is protected from modification in the presence of pretRNA but not mature tRNA (LaGrandeur *et al.*, 1994).

Extensive crosslinking and modification−interference data implicate the internal bulge connecting P15 and P16 in binding the 3′ CCA sequence of all pretRNAs (Knap *et al.*, 1990; B.-K.Oh and N.R.Pace, manuscript submitted; LaGrandeur *et al.*, 1994). These constraints are satisfied in both the molecular mechanics models and the manually refined structure; however, the specific contacts involved in the interaction remain speculative. One likely arrangement is that the pretRNA 3′ terminus interacts with one groove of an irregular helix formed by the P15−P16 internal loop. In the manually refined structure the CCA of the pretRNA is folded into the minor groove in an orientation consistent with both the intermolecular crosslinking and modification−interference data (Figure 6B).

The model is consistent with several studies indicating the importance of the tRNA TΨC loop in the recognition of pretRNA by RNase P RNA (Kahle *et al.*, 1990; Thurlow *et al.*, 1991; Holm and Krupp, 1992). Extensive intermolecular crosslinking from pretRNA G53 and G64 to the P7−P10 element of RNase P RNA (Table III; Nolan *et al.*, 1993) strongly suggests a role for this element in binding the end of the acceptor stem opposite the cleavage site. The precise nature of the contacts remains to be determined. The positioning of this portion of RNase P RNA relative to pretRNA is highly significant, as indicated by the low standard deviations for these helix positions in the molecular mechanics analysis. The orientation of these helices in the manually refined structure is consistent with the available crosslinking and comparative data (Figure 7).

The average positions of helices indicated by the molecular mechanics analysis and modeled in the manually refined interpretation are based on a sound but limited set of data. It is expected that the positions and orientations of the elements of the structural model will be revised as additional structural data become available. Continued intra- and intermolecular crosslinking can be used to probe the validity of this working model of the RNase P RNA−pretRNA complex. Additionally, comparisons of crosslinking results obtained from different bacterial

RNase P RNAs will help in refining the structure, and should suggest ways in which non-conserved sequences contribute to structural stability. Future experiments focused on individual points of contact between RNase P RNA and pretRNA will help define the precise nature of these interactions. The structural data and helical positions outlined in this study provide a basis on which to elaborate more detailed models of RNase P RNA structure. The model presented here provides a context in which to interpret such data and further explore how the structure of RNase P RNA reflects its chemistry and biology.

Materials and methods

Preparation of RNAs

cpRNAs were generated essentially as described by Nolan *et al.* (1993). Briefly, template DNAs for *in vitro* transcription were synthesized by PCR from tandemly repeated genes. The two primers define the endpoints of the PCR product and thus the 5′ and 3′ ends of the transcribed RNA. The upstream primer contained the core promoter for phage T7 RNA polymerase. PCRs contained 30 mM Tris−HCl, pH 8.3, 1 mM dNTPs, 50 mM potassium chloride, 1.5 mM magnesium chloride, 0.05% NP-40, 1–10 pg tandem RNase P RNA or tRNA genes and 100 pmol of the forward and reverse primers. The following primers were used: Ec63 forward, 5′-TAATACGACTCACTATAGGAAAGTCCGGGCTC-CACAG-3′; Ec63 reverse, 5′-TCCCCTCCGCCCGTCTCC-3′; Ec135 forward, 5′-TAATACGACTCACTATAGAGCAAACCGCCGATGG-3′; Ec135 reverse, 5′-TCTGTTGCACTGGTCGTG-3′; Ec179 forward, 5′-TAATACGACTCACTATAGAAAGGGTGCGGTAAGAGC-3′; Ec179 reverse, 5′-ACCCTTACCTGATCCCGC-3′; Ec229 forward, 5′-TAATA-CGACTCACTATAGGTAAACTCCACCCGGAGC-3′; Ec229 reverse, 5′-CCATTTGAGGTGGGCCTC-3′; Ec292 forward, 5′-TAATACGAC-TCACTATAGGTAGGCTGCTTGAGCC-3′; Ec292 reverse, 5′-CGGGT-TCAGTACGGGCCG-3′; Ec304 forward, 5′-TAATACGACTCACTA-TAGAGCCAGTGAGCGATTG-3′; Ec304 reverse, 5′-AAGCAGAATA-CCCGGGT-3′; Ec332 forward, 5′-TAATACGACTCACTATAGAATG-ACTGTCCACGACAG-3′; Ec332 reverse, 5′-ATCTAGGCCAGCAAT-CGC-3′; Ec350 forward, 5′-TAATACGACTCACTATAGAACCCGGC-TTATCGGTC-3′; Ec350 reverse, 5′-TGTCGTGGACAGTCATTC-3′; $tRNA^{Asp}$69 forward, 5′-TAATACGACTCACTATAGACCGCCAGGAT-CCCAA-3′; and $tRNA^{Asp}$69 reverse, 5′-CGGACGGGACTCGAACC-3′.

cpRNase P RNA genes were cloned in a specially constructed vector, pSBF, which contained *Bbs*I and *Fok*I restriction enzyme sites strategically positioned to cut at an upstream *Sma*I site. Cloning of these PCR DNAs into the *Sma*I site allowed the use of the *Fok*I or *Bbs*I sites to generate templates for *in vitro* transcription which were linearized precisely at the insert−vector junction.

The RNAs used in this study were prepared by *in vitro* transcription using phage T7 RNA polymerase. Non-radiolabeled RNAs were generated by transcription of 5–10 μg of template DNA with 40 U of phage T7 RNA polymerase in a 100 μl reaction containing 40 mM Tris−HCl pH 8.0, 1 mM spermidine, 5 mM dithiothreitol, 0.1% Triton X-100, 20 mM magnesium chloride and 2 mM NTPs for 5–12 h. For synthesis of RNAs containing a 5′ guanosine monophosphorothioate (GMPS) moiety the GTP concentration was reduced to 0.4 mM, and 2 mM GMPS were included in the reaction. Radiolabeled RNAs were generated by transcribing 1–2 μg of template DNA in a 40 μl reaction containing 50 μCi [α-^{32}P]GTP (3000 Ci/mmol, Amersham) and 0.25 mM GTP in addition to the buffers and reagents used in the transcription of non-radiolabeled RNAs. GMPS was synthesized as described (Burgin and Pace, 1990). RNase P RNAs were gel-purified by electrophoresis through 4% polyacrylamide/8 M urea gels; pretRNA was purified from 6% polyacrylamide/8 M urea gels. RNAs were visualized by UV shadow and passively eluted into 0.3 M sodium acetate, 20 mM Tris−HCl, pH 8.0, 1 mM ethylene diaminetetraacetate and 0.1% SDS. In the case of 5′ GMPS RNAs, 1 mM dithiothreitol was included in the elution buffer.

Analysis of RNase P enzymatic activity

cpRNase P RNAs were assayed for enzymatic activity in 10 μl reactions containing 1 nM RNase P RNA, 1 or 3 M ammonium acetate, 25 mM magnesium chloride, 40 mM Tris−HCl, pH 8.0, 0.1% SDS and 10 nM to 1 μM substrate pretRNA. Reactions were incubated for a length of time which effected no more that 20–30% cleavage of substrate (typically 5–10 min). Separation of substrate and cleaved products was accomplished by electrophoresis though 8% polyacrylamide/8 M urea gels. Gels were dried and conversion of pretRNA to cleaved products was analyzed using a Molecular Dynamics phosphorimaging system. The kinetic parameters k_{cat} and K_m were extracted by plotting velocity versus velocity/[substrate] (Eadie/Hofstee).

Photoaffinity crosslinking and mapping of crosslink sites

Crosslinking was accomplished essentially as described by Burgin and Pace (1990) and Nolan *et al.* (1993). An APA group was conjugated to the unique sulfur at the 5′ terminal phosphate of 5′ GMPS RNAs. For crosslinking, the conjugated RNA was incubated under *in vitro* RNase P assay conditions (described above) at 65°C for 2 min then 37°C for 10 min followed by exposure to 302 nM light at 25°C. Analytical reactions contained 2.00–0.02 nM 5′-APA cpRNase P RNA and were irradiated for 0.5–30.0 min. Preparative reactions contained 400 nM 5′-APA cpRNase P RNA and were irradiated for 30 min. pretRNA was included in the reactions as described in the figure legends. Calcium chloride replaced magnesium chloride in reactions containing pretRNA to suppress cleavage of the substrate (Smith and Pace, 1993).

RNA was recovered from crosslinking reactions by ethanol precipitation and the crosslinked species were resolved by electrophoresis through 4% polyacrylamide/8 M urea gels. RNAs were visualized by staining with ethidium bromide and excised from the gel. The various crosslinked species as well as the uncrosslinked RNA were eluted as described above. Crosslinked nucleotides were determined by primer extension of the crosslinked RNA as described previously (Burgin and Pace, 1990).

Computer modeling

Pseudo-atom models of *E.coli* RNase P RNA were generated using the YAMMP (Tan and Harvey, 1993) and YAMMP-RNA (Malhotra *et al.*, 1990; Malhotra and Harvey, 1994) suites of programs. In both molecular mechanics and manual refinement the bound tRNA was held in the appropriate 3-D conformation according to the crystallographically determined structure which was extracted from the Brookhaven Database, 1tra.pdb (Westhof and Sundaralingam, 1986). The 3-D coordinates of the resulting model are available by anonymous ftp at the following address ftp.bio.indiana.edu in the directory IUbio-Software+Data/mol-bio/rnase-p/threeD. A Silicon Graphics Personal Iris computer was used for molecular mechanics calculations and graphics. Manual model building was accomplished using the program MacroModel (Clark Still, Columbia University). Manually manipulated structures were refined further by energy minimization with YAMMP. Graphical display of the resulting structures was performed using the program RIBBONS (Carson, 1987).

Acknowledgements

We thank Tom LaGrandeur, Bong-Kyeong Oh, Dan Frank, Andrew Ellington and Steve Hajduk for many helpful discussions, and Don Gilbert for computer technical assistance. This work was supported by grants to N.R.P. from the National Institutes of Health (GM 34527) and to S.C.H. from the National Science Foundation (DMB-90-05767). M.E.H. was the recipient of an NIH post-doctoral fellowship (GM 15979). J.W.B. was supported by an Institute Fellowship for Molecular and Cellular Biology from Indiana University.

References

Altman,S., Kirsebom,L. and Talbot,S. (1993) *FASEB J.*, **7**, 7–14.

Brimacombe,R., Atmadja,J., Stiege,W. and Schuler,D. (1988) *J. Mol. Biol.*, **199**, 115–136.

Brown,J.W., Haas,E.S., James,B.D., Hunt,D.A., Liu,J. and Pace,N.R. (1991) *J. Bacteriol.*, **173**, 3855–3863.

Burgin,A.B. and Pace,N.R. (1990) *EMBO J.*, **9**, 4111–4118.

Carson,M. (1987) *J. Mol. Graph.*, **5**, 103–106.

Cech,T.R. (1993) In Gesteland,R.F. and Atkins,J.F. (eds), *The RNA World.* Cold Spring Harbor Laboratory Press, Cold Spring Harbor, NY, pp. 239–269.

Cooper,J.P. and Hagerman,P.J. (1989) *J. Mol. Biol.*, **198**, 711–719.

Doudna,J.A., Grosshans,C., Gooding,A. and Kundrot,C.E. (1993) *Proc. Natl Acad. Sci. USA*, **90**, 7829–7833.

Gauss,D.H., Grüter,F. and Sprinzl,M. (1979) In Schimmel,P.A., Söll,D. and Abelson,J.N. (eds), *Transfer RNA: Structure, Properties and Recognition.* Cold Spring Harbor Laboratory Press, Cold Spring Harbor, NY, pp. 518–522.

Guerrier-Takada,C. and Altman,S. (1992) *Proc. Natl Acad. Sci. USA*, **89**, 1266–1270.
Guerrier-Takada,C., Gardiner,K., Marsh,T., Pace,N. and Altman,S. (1983) *Cell*, **35**, 849–857.
Haas,E.S., Brown,J.W., Pitulle,C. and Pace,N.R. (1994) *Proc. Natl Acad. Sci. USA*, **91**, 2527–2531.
Heus,H. and Pardi,A. (1991) *Science*, **253**, 191–194.
Hixson,S.H. and Hixson,S.S. (1975) *Biochemistry*, **14**, 4251–4254.
Holbrook,S.R., Cheong,C., Tinoco,I.,Jr and Kim,S.-H. (1991) *Nature*, **353**, 579–581.
Holm,P.S. and Krupp,G. (1992) *Nucleic Acids Res.*, **20**, 421–423.
James,B.D., Olsen,G.J., Liu,J.S. and Pace,N.R. (1988) *Cell*, **52**, 19–26.
Kahle,D., Wehmeyer,U. and Krupp,G. (1990) *EMBO J.*, **9**, 1927–1937.
Kim,S.-H., Suddath,F.L., Quigley,G.L., McPherson,A., Sussman,J.L., Wang,A.H.J., Seeman,N.C. and Rich,A. (1974) *Science*, **185**, 435–440.
Knap,A.K., Wesolowski,D. and Altman,S. (1990) *Biochimie*,**72**, 779–790.
LaGrandeur,T.E., Hüttenhofer,A., Noller,H.F. and Pace,N.R. (1994) *EMBO J.*, **13**, 3953–3963.
Malhotra,A. and Harvey,S.C. (1994) *J. Mol. Biol.*, **240**, 308–340.
Malhotra,A., Tan,R.K.-Z. and Harvey,S.C. (1990) *Proc. Natl Acad. Sci. USA*, **87**, 1950–1954.
Malhotra,A., Tan,R.K.-Z. and Harvey,S.C. (1994) *Biophys. J.*, **66**, 1777–1795.
Michel,F. and Westhof,E. (1990) *J. Mol. Biol.*, **216**, 585–610.
Milligan,J.F. and Uhlenbeck,O.C. (1989) *Methods Enzymol.*, **180**, 51–62.
Moras,D., Comarmond,M.B., Fischer,J., Weiss,R., Thierry,J.C., Ebel,J.P. and Giege,R. (1980) *Nature*, **288**, 669–674.
Murchie,A.I.H., Clegg,R.M., von Kitzing,E., Dickett,D.R., Diekmann,S. and Lilley,D.M.J. (1989) *Nature*, **341**, 763–766.
Neumann,H. and Smith,R.A. (1967) *Arch. Biochem. Biophys.*, **122**, 354–361.
Nolan,J.M., Burke,D.H. and Pace,N.R. (1993) *Science*, **261**, 762–765.
Puglisi,J.D., Wyatt,J.R. and Tinoco,I. (1990) *J. Mol. Biol.*, **214**, 437–453.
Reich,C., Gardiner,K., Pace,B., Olsen,G.J., Marsh,T.L. and Pace,N.R. (1986) *J. Biol. Chem.*, **261**, 7888–7893.
Reich,C., Olsen,G.J., Pace,B. and Pace,N.R. (1988) *Science*, **239**, 178–181.
Robertus,J.D., Ladner,J.E., Finch,J.R., Rhodes,D., Brown,R.S., Clark,B.F.C. and Klug,A. (1974) *Nature*, **250**, 546–551.
Schuster,G.G. and Platz,M.S. (1992) In Volman,D., Hammond,G. and Neckers,D. (eds), *Advances in Photochemistry*. John Wiley and Sons, New York, Vol. 12, pp. 70–141.
Smith,D. and Pace,N.R. (1993) *Biochemistry*, **32**, 5273–5281.
Stern,S., Weiser,B. and Noller,H.F. (1988) *J. Mol. Biol.*, **204**, 448–481.
Tallsjö,A. and Kirsebom,L.A. (1993) *Nucleic Acids Res.*, **21**, 51–67.
Tan,R.K.-Z. and Harvey,S.C. (1993) *J. Comp. Chem.*, **14**, 455–470.
Thurlow,D.L., Shilowski,D. and Marsh,T. (1991) *Nucleic Acids Res.*, **19**, 885–891.
Varani,G., Cheong,C. and Tinoco,I.,Jr (1991) *Biochemistry*, **30**, 3280–3289.
Waugh,D.S. and Pace,N.R. (1993) *FASEB J.*, **7**, 188–195.
Westhof,E. and Sundaralingam,M. (1986) *Biochemistry*, **25**, 4868–4875.
Westhof,E., Dumas,P. and Moras,D. (1985) *J. Mol. Biol.*, **184**, 119–145.
Westhof,E., Romby,P., Romaniuk,P.J., Ebel,J.-P., Ehresmann,C. and Ehresmann,B. (1989) *J. Mol. Biol.*, **184**, 417–431.
Wimberly,B., Varani,G. and Tinoco,I.,Jr (1993) *Biochemistry*, **32**, 1078–1087.

Received on May 12, 1994; revised on June 14, 1994